TWO-POINT ENERGY AND ENSTROPHY BUDGETS IN TURBULENT BOUNDARY LAYERS

Gabriele Boga
Dipartimento di Ingegneria Enzo Ferrari (DIEF)
Università di Modena e Reggio Emilia
Via P. Vivarelli 10, 41125, Modena, Italy
gabriele.boga@unimore.it

Andrea Cimarelli
Dipartimento di Ingegneria Enzo Ferrari (DIEF)
Università di Modena e Reggio Emilia
Via P. Vivarelli 10, 41125, Modena, Italy

ABSTRACT

The present contribution addresses the multiscale phenomena involving the energy and enstrophy dynamics in wall-turbulent flows. The flow configuration chosen is that of a temporally evolving boundary layer up to a friction Reynolds number $Re_\tau = 1500$. The presence of a solid wall results in a confinement of the dynamics, significantly modifying the classical picture of turbulence, in which the prominent feature of turbulence is the energy transfer from large to small scales which is described by a single scalar quantity: the average dissipation rate. These topics are investigated through the second-order structure function formalism applied to both velocity and vorticity. The results obtained on the boundary layer highlight the presence of a split energy and enstrophy interscale transfer that feeds scales that are both larger and smaller with respect to the scale at which energy is injected. The tool used proved effective in capturing such phenomena.

INTRODUCTION

Wall-turbulent flows are of great interest for a variety of industrial and environmental applications. Their dynamics are governed by the combined role of inner and outer self-sustaining mechanisms involving different scale motions (Jiménez & Pinelli, 1999; Mizuno & Jiménez, 2013). The near-wall region is the site of a high rate of turbulent energy production, and its dynamics are governed by motions scaling in inner units. On the other hand, for high Reynolds numbers, the outer overlap layer is thought to become relevant, being the site of self-sustaining mechanisms of large flow structures following mixed inner/outer scaling. The complex interactions involved, which determine the overall momentum and heat transfer, are not yet fully understood, and their understanding underpins the development of more reliable turbulence models and new control strategies. The strong inhomogeneity and anisotropy imposed by the presence of the wall deeply modify the classical picture of turbulence. The near-wall region is in fact the site of a strong reverse energy transport process in the wall-parallel directions, feeding long and wide scales that dissipate energy through sharp gradients in the wall-normal direction. A similar scenario, albeit more moderate in intensity, is observed in the Turbulent/Non-Turbulent Interface (TNTI) region (see da Silva *et al.* (2014) for a comprehensive review). In this context, turbulent enstrophy (defined as $\zeta = \omega_i \omega_i$, where $\omega = \nabla \times u$ is the fluctuating vorticity and u_i is the fluctuating velocity) is an observable of great interest. In fact, given its connection with both dissipation and with the energy cascade (through the vortex stretching mechanism), it can give us further insight in regions of the flow characterised by a confined dynamics as the near-wall and TNTI regions mentioned above.

In the present work, we make use of two-point statistics of both turbulent kinetic energy and turbulent enstrophy to investigate the phenomena mentioned above. The analyses are conducted on the flow configuration of a temporally evolving boundary layer, characterized by the simultaneous presence of a solid wall and of a free TNTI that propagates via the entrainment phenomenon. The simulation settings and the flow configuration are briefly described in the following section. Subsequently, the two-point formalism applied to the turbulent energy and enstrophy is presented, along with some relevant results obtained. The paper is concluded with some final remarks in the last section.

FLOW SETTINGS

The flow configuration chosen in the present work is that of the temporal boundary layer, which consists of an initially stationary fluid with a flat wall at the bottom that moves with a constant velocity U_w. Periodic boundary conditions are imposed in the streamwise x and spanwise y directions. In the wall-normal direction z a Dirichlet boundary condition $(u, v, w) = (U_w, 0, 0)$ is imposed at the bottom of the domain $z = 0$, while a free-slip boundary condition is used at the top of the domain $\partial u/\partial z = 0$, $(v, w) = (0, 0)$. The direct numerical simulations have been performed using the code CaNS (Costa, 2018) that employs a standard pressure-projection method and a staggered second-order finite-difference scheme for spatial discretization. In the present simulations, time integration is performed using a mixed approach. The viscous terms in the wall-normal direction are integrated implicitly with a

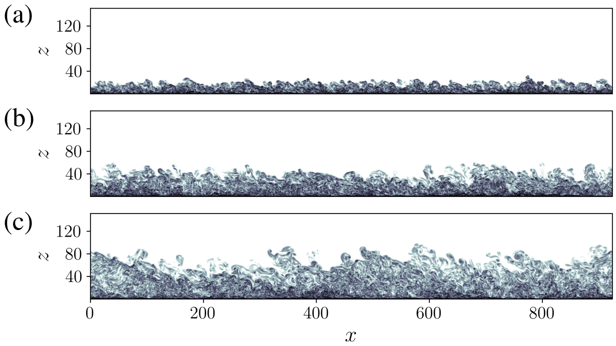

Figure 1. Slices of spanwise vorticity module $|\omega_y|$ at three different time instants corresponding to $Re_\tau = 500$ (a), 1000 (b) and 1500 (c). Darker colour indicates a greater intensity.

Crank–Nicholson scheme, while all the other terms are integrated explicitly using a three-step Runge–Kutta method with a condition $CFL = 0.95$.

As shown in figure 1, this flow evolves in time rather than in space, thus recovering the statistical homogeneity in the streamwise direction. For this reason, this flow configuration allows us to obtain a simplified problem with respect to the spatially evolving boundary layer. In the temporal boundary layer the friction Reynolds number, defined as $Re_\tau = u_\tau \delta/\nu$ -where u_τ is the friction velocity, ν is the kinematic viscosity and δ is the boundary layer thickness-, increases in time and its evolution is reported in figure 2(a). All the results presented in the following are relative to the last time instant of the direct numerical simulation conducted, corresponding to $Re_\tau = 1500$.

Despite the different configuration, the temporal boundary layer has been shown to qualitatively capture the same physical mechanisms as the spatial boundary layer (Kozul *et al.*, 2016; Cimarelli *et al.*, 2024*a*; Zhang *et al.*, 2018). Most of the classical results are also recovered, such as the evolution of the friction coefficient $C_f \approx 0.024 Re_\theta^{-1/4}$, reported in figure 2(a) in dotted line, and the shape of the mean velocity profile, shown in figure 2(b) together with its diagnostic function $\Xi(z) = z^+ \partial U^+/\partial z^+$.

At the final time instant, the domain size with respect to the boundary layer thickness is $(L_x, L_y, L_z) = (11.9, 5.9, 2.8)\delta$ discretized in $(N_x, N_y, N_z) = (3072, 3072, 768)$ in the streamwise x, spanwise y and wall-normal z directions respectively. This discretization results in a resolution of $(\Delta x^+, \Delta y^+) = (5.8, 2.9)$ in the statistically homogeneous directions and $(\Delta z_w^+, \Delta z_\delta^+, (\Delta z/\eta)_\delta) = (0.09, 9.17, 1.13)$ in the wall-normal direction, where the subscripts $\cdot_w$ and $\cdot_\delta$ indicate quantities evaluated at the wall $z = 0$ and at $z = \delta$ respectively, the superscript $\cdot^+$ indicates quantities normalized in wall units and η is the Kolmogorov scale.

In the following, the classical Reynolds decomposition is used, denoted as $u_i^* = U_i + u_i$, where u_i^* is the total velocity, while $U_i = \langle u_i^* \rangle$ and u_i are the mean and fluctuating velocities, respectively. In the present work, the average operation, indicated with $\langle \cdot \rangle$, is computed by spatial averaging in the wall-parallel homogeneous directions, x and y, and by ensemble averaging between four indipendent realizations of the flow.

TWO-POINT FORMALISM

The multiscale nature of the topics mentioned in the introduction makes it necessary to use a tool capable of distinguishing between the different scales of motion. In the present work, we use the formalism provided by the second-order structure function. For a generic vector field f, the second-order structure function is defined as $\delta f^2(\boldsymbol{x}_c, \boldsymbol{r}, t) = \delta f_i \delta f_i$, being $\delta f_i = f_i(\boldsymbol{x''}, t) - f_i(\boldsymbol{x'}, t)$ the two-point increment, $\boldsymbol{x_c} = 1/2\left(\boldsymbol{x'} + \boldsymbol{x''}\right)$ the midpoint and $\boldsymbol{r} = \boldsymbol{x''} - \boldsymbol{x'}$ the separation vector.

Energy

Applying this framework to the Navier-Stokes equations it is possible to derive the generalized Kolmogorov equation (Hill, 2002) that describes the evolution of the average "scale-energy" $\langle \delta q^2 \rangle = \langle \delta u_i \delta u_i \rangle$. For the symmetries of the temporal boundary layer, this equation reads:

$$\frac{\partial \langle \delta q^2 \rangle}{\partial t} = T_r + D_r + T_c + \Pi - 4\langle \widetilde{\varepsilon} \rangle \tag{1}$$

with:

$$\begin{aligned} T_r &= -\frac{\partial \langle \delta q^2 \rangle \delta U}{\partial r_x} - \frac{\partial \langle \delta q^2 \delta u_i \rangle}{\partial r_i}, \quad D_r = 2\nu \frac{\partial^2 \langle \delta q^2 \rangle}{\partial r_i \partial r_i}, \\ T_c &= -\frac{\partial \langle \delta q^2 \widetilde{w} \rangle}{\partial z_c} - \frac{2}{\rho}\frac{\partial \langle \delta p \delta w \rangle}{\partial z_c} + \frac{\nu}{2}\frac{\partial^2 \langle \delta q^2 \rangle}{\partial {z_c}^2}, \\ \Pi &= -2\langle \delta u \delta w \rangle \widetilde{\left(\frac{\partial U}{\partial z}\right)} - 2\langle \delta u \widetilde{w} \rangle \delta \left(\frac{\partial U}{\partial z}\right) \end{aligned} \tag{2}$$

where T_r and D_r represent the inertial and diffusive transports in the space of scales, T_c is the total transport in the physical space, Π is the production term, $\varepsilon = \partial u_i/\partial x_j \partial u_i/\partial x_j$ is the turbulent kinetic energy dissipation and $\widetilde{f_i} = 1/2(f_i' + f_i'')$ is the two-point average.

This equation can be rewritten in its conservative form, highlighting the source terms and the fluxes:

$$\frac{\partial \langle \delta q^2 \rangle}{\partial t} + \boldsymbol{\nabla_4} \cdot \boldsymbol{\phi} = S \tag{3}$$

thus emphasizing that the generalized Kolmogorov equation represents an exact formalism for the study of the hyperflux of scale-energy in the compound space of scales through the three-dimensional flux ϕ_{r_i} and physical space through the one-dimensional flux ϕ_{c_z}

$$\begin{aligned} \phi_{r_i} &= \langle \delta q^2 \delta u_i \rangle + \langle \delta q^2 \delta U \rangle \delta_{i1} - 2\nu \frac{\partial \langle \delta q^2 \rangle}{\partial r_i}, \\ \phi_{c_z} &= \langle \delta q^2 \widetilde{w} \rangle + \frac{2}{\rho}\langle \delta p \delta w \rangle - \frac{\nu}{2}\frac{\partial \langle \delta q^2 \rangle}{\partial z_c} \end{aligned} \tag{4}$$

from the production to the dissipation regions of the augmented space of turbulence identified by the source term

$$S = \Pi - 4\langle \widetilde{\varepsilon} \rangle \tag{5}$$

Enstrophy

Analogously, by applying the two-point formalism to the vorticity equation, we obtain the two-point enstrophy budget, describing the evolution of $\langle \delta \zeta^2 \rangle = \langle \delta \omega_i \delta \omega_i \rangle$ (see Baj *et al.*

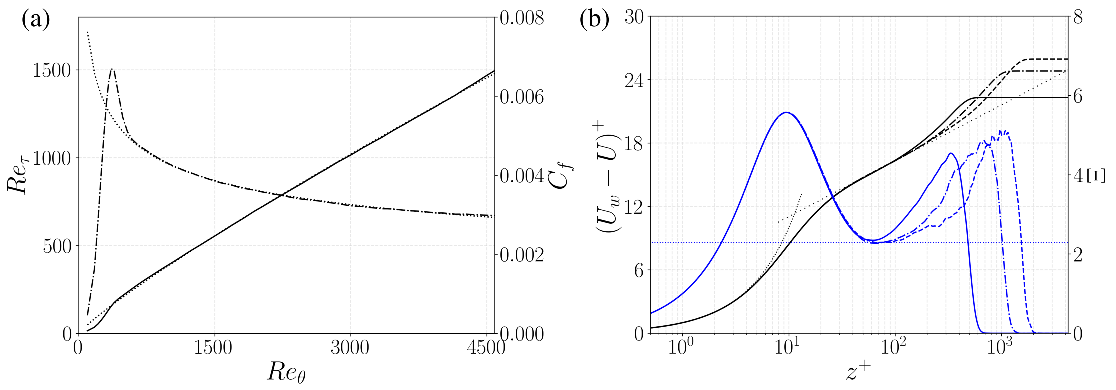

Figure 2. (a) Evolution of the friction Reynolds number Re_τ (solid line) and of the friction coefficient C_f (dash-dotted line) with the momentum-thickness Reynolds number Re_θ. (b) Mean velocity profiles $(U_w - U)$ (black lines) and relative diagnostic function Ξ (blue lines) at different time instants corresponding to friction Reynolds number of $Re_\tau = 500$ (solid lines), $Re_\tau = 1000$ (dash-dotted lines) and 1500 (dashed lines). The linear and logarithmic behaviour are reported in dotted lines.

(2022); Boga (2025) for further details), which for the symmetries of the temporal boundary layer reads:

$$\frac{\partial \langle \delta\zeta^2 \rangle}{\partial t} = T_{r_\zeta} + D_{r_\zeta} + T_{c_\zeta} + \xi + \Pi_\zeta - 4\langle \chi \rangle \qquad (6)$$

with:

$$\begin{aligned}
T_{r_\zeta} &= -\frac{\partial \langle \delta\zeta^2 \rangle \delta U}{\partial r_x} - \frac{\partial \langle \delta\zeta^2 \delta u_j \rangle}{\partial r_j}, \\
D_{r_\zeta} &= 2\nu \frac{\partial^2 \langle \delta\zeta^2 \rangle}{\partial r_j \partial r_j}, \\
T_{c_\zeta} &= -\frac{\partial \langle \delta\zeta^2 \widetilde{w} \rangle}{\partial z_c} + \frac{\nu}{2}\frac{\partial^2 \langle \delta\zeta^2 \rangle}{\partial z_c^2}, \\
\xi &= 2\widetilde{\Omega}_y \langle \delta\omega_i \delta\left(\frac{\partial u_i}{\partial y}\right)\rangle + 2\delta\Omega_y \langle \delta\omega_i \widetilde{\left(\frac{\partial u_i}{\partial y}\right)}\rangle \\
&+ 2\langle \delta\omega_x \widetilde{\omega}_z \rangle \delta\left(\frac{\partial U}{\partial z}\right) + 2\langle \delta\omega_x \delta\omega_z \rangle \widetilde{\left(\frac{\partial U}{\partial z}\right)} + \\
&2\langle \delta\omega_i \widetilde{\omega}_j \delta\left(\frac{\partial u_i}{\partial x_j}\right)\rangle + 2\langle \delta\omega_i \delta\omega_j \widetilde{\left(\frac{\partial u_i}{\partial x_j}\right)}\rangle, \\
\Pi_\zeta &= -2\langle \delta\omega_y \widetilde{w} \rangle \delta\left(\frac{\partial \Omega_y}{\partial z}\right) - 2\langle \delta\omega_y \delta w \rangle \widetilde{\left(\frac{\partial \Omega_y}{\partial z}\right)}
\end{aligned} \qquad (7)$$

where T_{r_ζ} and D_{r_ζ} are the inertial and diffusive enstrophy transports in the space of scales, T_{c_ζ} is the enstrophy transport in the physical space, Π_ζ is the enstrophy production via mean vorticity gradients, ξ is the vortex stretching term and $\chi = \partial\omega_i/\partial x_j \partial\omega_i/\partial x_j$ is the enstrophy destruction.

The conservative form of the two-point enstrophy budget reads:

$$\frac{\partial \langle \delta\zeta^2 \rangle}{\partial t} + \boldsymbol{\nabla}_\mathbf{4} \cdot \boldsymbol{\phi}_\zeta = S_\zeta \qquad (8)$$

with

$$\begin{aligned}
\phi_{\zeta_{r_i}} &= \langle \delta\zeta^2 \delta u_i \rangle + \langle \delta\zeta^2 \delta U \rangle \delta_{i1} - 2\nu \frac{\partial \langle \delta\zeta^2 \rangle}{\partial r_i}, \\
\phi_{\zeta_{c_z}} &= \langle \delta\zeta^2 \widetilde{w} \rangle - \frac{\nu}{2}\frac{\partial \langle \delta\zeta^2 \rangle}{\partial z_c}
\end{aligned} \qquad (9)$$

being the fluxes in the space of scales and in the physical space respectively, and

$$S_\zeta = \Pi_\zeta + \xi - 4\langle \widetilde{\chi} \rangle \qquad (10)$$

being the source term.

PRELIMINARY RESULTS

In the present work, we limit the analysis of the two-point energy and enstrophy budgets (equations 1 and 6) to the subspace $r_z = 0$, hence expanding the fluxes and sources of energy and enstrophy only in the streamwise and spanwise scales, r_x and r_y, in addition to the wall-normal direction z_c. This simplification reduces the dimensionality of the problem and allows us to get a first insight into the two-point dynamics without having to deal with the 4-dimensional space (z_c, r_x, r_y, r_z), which is more comprehensive, but also more difficult to handle and visualize.

For simplicity, we start by comparing the energy and enstrophy dynamics by further limiting the problem to the subspace $r_x = r_z = 0$, thus investigating the spanwise dynamics on the plane $(z_c, r_y)_{|r_x=r_z=0}$ (see Cimarelli *et al.* (2024*a*,*b*) for the two-point energy budget in both the $(z_c, r_x, r_y)_{|r_z=0}$ and $(z_c, r_y)_{|r_x=r_z=0}$ subspaces). In figure 3 the energy and enstrophy net source terms and fluxes, are reported as contours and black arrows on the $(z_c, r_y)_{|r_x=r_z=0}$ plane in the near-wall region. In this region, the energy and enstrophy net sources S and S_ζ exhibit some qualitative similarities, showing a high production rate in the buffer layer and an intense dissipation region in the viscous sublayer, together with a more moderate dissipation region at small scales r_y^+, i.e. near the vertical axis. The energy and enstrophy fluxes ϕ and ϕ_ζ show that the spanwise dynamics is governed by a split energy and enstrophy cascade feeding scales both larger and smaller than the scale at which energy is injected. In this representation, the arrows tilting towards the left indicate a flux towards smaller scale, hence a direct energy (or enstrophy) transfer, while arrows tilting toward the right indicate an average reverse transfer.

A substantial difference between the turbulent kinetic energy and the turbulent enstrophy is that, while the first originates from the buffer layer and is then transported away and towards the wall, enstrophy is generated at the wall through shear and is injected into the domain via diffusion through the

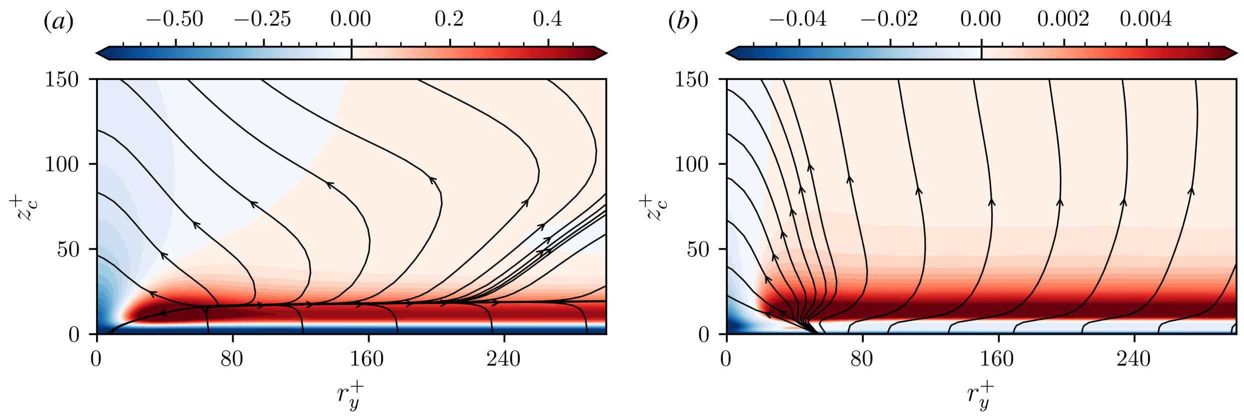

Figure 3. (a) Source S^+ and fluxes ϕ^+ of $\langle \delta q^2 \rangle$ and (b) source S_ζ^+ and fluxes $\phi_\zeta{}^+$ of $\langle \delta \zeta^2 \rangle$ in the near-wall region reported in the subspace $(r_y^+, z_c^+)|_{r_z, r_x=0}$. Negative source values ($S^+ < 0$ and $S_\zeta^+ < 0$) are reported on scale of blues, while positive source values ($S^+ > 0$ and $S_\zeta^+ > 0$) on scale of reds. The fluxes $((\phi_{r_y}^+, \phi_{c_z}^+)(r_y^+, z_c^+)$ in (a) and $(\phi_{\zeta_{r_y}}^+, \phi_{\zeta_{c_z}}^+)(r_y^+, z_c^+)$ in (b)) are represented by lines and arrows.

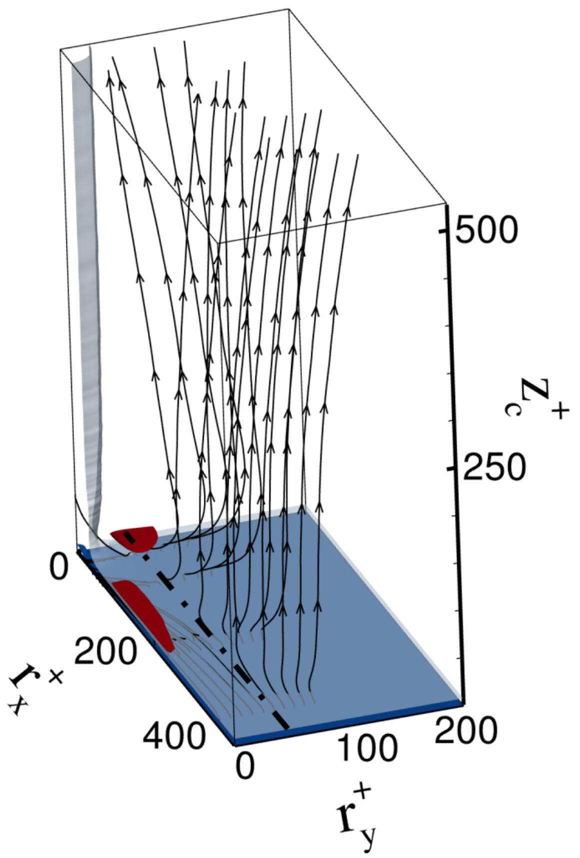

Figure 4. Sources and fluxes of $\langle \delta \zeta^2 \rangle$ in the subspace $(r_x, r_y, z_c)|_{r_z=0}$. Isosurfaces of positive net source of enstrophy $S_\zeta^+ = 0.008$ (red) and negative net source $S_\zeta^+ = -0.05$ (solid blue) and $S_\zeta^+ = -5 \times 10^{-6}$ (transparent grey). The fluxes $\boldsymbol{\phi}_\zeta$ are reported as black lines and arrows.

boundary enstrophy flux (see Lighthill (1963); Eyink (2008); Terrington *et al.* (2021, 2023); Kumar *et al.* (2023) for a comprehensive overview). Since enstrophy is generated at the wall by shear, it is initially composed solely by its streamwise and spanwise contributions. As it diffuses into the region immediately adjacent to the wall, enstrophy is also partially dissipated, mainly by wall-normal gradients. Enstrophy is then transported away from the wall and amplified mainly via vortex stretching, with a peak of activity in the buffer layer, as shown in figure 3(b). The vortex stretching term ξ is also responsible for the redistribution of enstrophy through its streamwise, spanwise and wall-normal contribution through the vortex tilting mechanism. The picture that emerges by expanding the view to the r_x dimension (hence investigating the $(z_c, r_x, r_y)_{|r_z=0}$ dynamics), as shown in figure 4, appears to show qualitatively the same picture as that described by the spanwise dynamics (in figure 3(b)), with the addition of a transfer of entropy towards smaller streamwise r_x scales. More results on the two-point enstrophy dynamics can be found in Boga (2025).

CONCLUSIONS

In the present paper, we make use of the theoretical framework provided by the two-point formalism in order to investigate the analysis of the energy and enstrophy dynamics in an augmented space of scales and position. This tool allows us to obtain information on the multiscale features of the turbulent flow analysed, i.e. a temporal boundary layer at a friction Reynolds number $Re_\tau = 1500$. Some preliminary results are presented, highlighting the potential of this tool for studying topics related to the energy and enstrophy interscale transfer, production and dissipation mechanisms, particularly in regions affected by the confinement effect introduced by the presence of a wall or of a TNTI.

ACKNOWLEDGEMENTS

This work was supported by the Italian Ministry of University and Research (MUR), through the PRIN 2022 PNRR Project 20224NY2YK - ADMIRE - “ADvanced Modeling of hIgh-speed aerodynamics for MaRs Entry”, CUP E53C24002710006, funded by the National Recovery and Resilience Plan (PNRR), Italy, Mission 04 Component 2 Investment 1.1.

REFERENCES

Baj, P., Alves Portela, F. & Carter, D.W. 2022 On the simultaneous cascades of energy, helicity, and enstrophy in incompressible homogeneous turbulence. *J. Fluid Mech.* **952**, A20.

Boga, G. 2025 Multiscale phenomena in turbulent boundary layers. PhD thesis, Corso di Dottorato di Ricerca in Ingegneria Industriale e del Territorio "Enzo Ferrari" - XXXVII Ciclo.

Cimarelli, A., Boga, G., Pavan, A., Costa, P. & Stalio, E. 2024*a* Energy cascade phenomena in temporal boundary layers. *Flow Turb. Comb.* **112**, 129–145.

Cimarelli, A., Boga, G., Pavan, A., Costa, P. & Stalio, E. 2024*b* Spatially evolving cascades in wall turbulence with and without interface. *J. Fluid Mech.* **987**, A4.

Costa, P. 2018 A FFT-based finite-difference solver for massively-parallel direct numerical simulations of turbulent flows. *Comput. & Math. App.* **76** (8), 1853–1862.

da Silva, C. B., Hunt, J. C. R., Eames, I. & Westerweel, J. 2014 Interfacial layers between regions of different turbulence intensity. *Annu. Rev. Fluid Mech.* **46**, 567–590.

Eyink, G. L. 2008 Turbulent flow in pipes and channels as cross-stream "inverse cascades" of vorticity. *Phys. Fluids* **20** (12), 125101.

Hill, R.J. 2002 Exact second-order structure-function relationship. *J. Fluid Mech.* **468**, 317–326.

Jiménez, J. & Pinelli, A. 1999 The autonomous cycle of near-wall turbulence. *J. Fluid Mech.* **389**, 335–359.

Kozul, M., Chung, D. & Monty, J. P. 2016 Direct numerical simulation of the incompressible temporally developing turbulent boundary layer. *J. Fluid Mech.* **796**, 437–472.

Kumar, S., Meneveau, C. & Eyink, G. 2023 Vorticity cascade and turbulent drag in wall-bounded flows: plane poiseuille flow. *J. Fluid Mech.* **974**, A27.

Lighthill, M.J. 1963 Introduction: boundary layer theory. In *Laminar Boundary Layers* (ed. L. Rosenhead). Oxford University Press.

Mizuno, Y. & Jiménez, J. 2013 Wall turbulence without walls. *J. Fluid Mech.* **723**, 429–455.

Terrington, S.J., Hourigan, K. & Thompson, M.C. 2021 The generation and diffusion of vorticity in three-dimensional flows: Lyman's flux. *J. Fluid Mech.* **915**, A106.

Terrington, S.J., Hourigan, K. & Thompson, M.C. 2023 The lyman–huggins interpretation of enstrophy transport. *J. Fluid Mech.* **958**, A30.

Zhang, X., Watanabe, T. & Nagata, K. 2018 Turbulent/nonturbulent interfaces in high-resolution direct numerical simulation of temporally evolving compressible turbulent boundary layers. *Phys. Rev. Fluids* **3**, 094605.